Journal of Alloys and Compounds 501 (2010) 366–370

Contents lists available at ScienceDirect

Journal of Alloys and Compounds

journal homepage: www.elsevier.com/locate/jallcom

Study on the intermetallic phases in the Mg–Ce system Part II. Diffusion couple investigation

X. Zhang, D. Kevorkov, M.O. Pekguleryuz*

Materials Engineering, McGill University, Montreal, Quebec, Canada H3A 2B2

ARTICLE INFO

Article history:
Received 3 February 2010
Received in revised form 10 April 2010
Accepted 14 April 2010
Available online 22 April 2010

Keywords:
Magnesium
Cerium
Phase diagram
Diffusion couple

ABSTRACT

Mg–Ce diffusion couple annealed at 400 °C was investigated via electron probe microanalysis (EPMA), and scanning electron microscopy/energy dispersive spectroscopy (SEM/EDS). The results validated the compositions of the intermetallic phases experimentally determined by Zhang et al. [1] on the Mg-rich side of the binary phase diagram and refined the phase diagram suggested by Zhang et al. [2] for the composition range of 38–70 wt% Ce. A revised equilibrium phase diagram was proposed for the Mg–Ce system up to 50 at% Ce.

1. Introduction

Magnesium alloys containing rare earth (RE) elements have attracted considerable interest from the transport industry because of their elevated-temperature performance [3–5]. RE elements are usually alloyed to magnesium as mischmetal (Mm) where Mm is a natural mixture of 50% cerium with the reminder being mainly lanthanum and neodymium or as didymium which is a mixture of praseodymium and neodymium. The different effects of individual RE metals on the properties of Mg have been demonstrated in several studies [6–8]. This may be explained by the different solid solubilities of RE elements in Mg and the different compounds formed in each Mg–RE system [9].

The Mg–Ce phase diagram [1,2,9] exhibits six intermetallic compounds that are formed from the liquid by peritectic reactions, except for Mg_3Ce that melts congruently. The alloy systems are described in detail in [10].

1.1. Mg-rich side (<15 at% Ce)

Rokhlin [10] discussed that some uncertainty existed in the region of the three intermetallics, $Mg_{12}Ce$, $Mg_{10.3}Ce$ and $Mg_{41}Ce_5$. When Vogel studied the system, the Mg_9Ce phase was postulated for this region due to the similarity between magnesium–cerium and the magnesium–lanthanum diagrams [2,11], until Wood and Cramer [12] determined three compounds that formed peritectically ($Mg_{12}Ce$, $Mg_{17}Ce_2$, $Mg_{8.25}Ce$) in this composition range.

The analysis of the lattice parameters of $Mg_{17}Ce_2$ [10] demonstrated that the compound can be Mg-enriched and deviate from the stoichiometric composition of $Mg_{17}Ce_2$. It was described by the formula $Mg_{10.3}Ce$ which is not convincing since there was no accompanying metallography or X-ray diffraction (XRD) study as discussed by Rokhlin [10] who investigated the $Mg_{12}Ce$ composition range and, based on the fact that the $Mg_{12}Ce$ is considerably enriched in Ce (up to $Mg_{9.6}Ce$), concluded that the formula $Mg_{10.3}Ce$ cannot be assigned to the subsequent compound [10,p. 27]. Thermal analysis investigation of this region by Saccone et al. [13] has revealed thermal arrests for the 9–10 at% Ce region in the 610–623 °C interval and confirmed the invariant reactions in the phase diagram given in [14]; however, the authors used the $Mg_{10.3}Ce$ designation without presenting the specific electron probe microanalysis (EPMA) results. Zhang et al. [1] have recently determined via XRD and EPMA that $Mg_{12}Ce$ was enriched in Ce and the compound was re-designated as $Mg_{11}Ce$; also, the $Mg_{10.3}Ce$ compound was eliminated from the suggested phase diagram [1] until further study.

The compound initially assumed to be $Mg_{8.25}Ce$, was subsequently assigned the formula $Mg_{42}Ce_5$ based on the crystal structure; it was later replaced with $Mg_{41}Ce_5$. Zhang et al. have redesignated the $Mg_{41}Ce_5$ phase as $Mg_{39}Ce_5$ in their previous study [1]. The $Mg_{11}Ce$ and $Mg_{39}Ce_5$ were considered to be vacancy defect structures of $Mg_{12}Ce$ and $Mg_{41}Ce_5$, respectively, where certain Mg sites may be occupied by vacancies to keep the e/a ratio per unit cell and maintain compound stability [15].

* Corresponding author.
E-mail address: mihriban.pekguleryuz@mcgill.ca (M.O. Pekguleryuz).

0925-8388/$ – see front matter © 2010 Elsevier B.V. All rights reserved.
doi:10.1016/j.jallcom.2010.04.107

1.2. Ce-rich side (>15 at% Ce)

The binary compounds Mg_3Ce, Mg_2Ce and MgCe that exist in this range are considered to be well established [10]. In 2007, Zhou et al. [16] determined the electronic structure and the stability of the Mg–Ce intermetallic compounds, Mg_3Ce, Mg_2Ce, MgCe, $MgCe_2$, $MgCe_3$, from first principle calculations and found that, based on cohesive energies, the structural stabilities of D03-Mg_3Ce and of C15-Mg_2Ce are high and hence these compounds would exist even in Mg-rich alloys. This would explain why the Mg_3Ce was found in Mg-rich alloys investigated by the present authors in their previous study [2]. X-ray absorption study on Mg_2Ce by Grandjean et al. [17] sheds light on cerium valency in this compound; it was found that there is very little hybridization between the Ce – 4f and the Mg – 3s orbitals resulting in trivalent cerium valency.

The compounds that are rich in Ce are currently being investigated for magnetic, electronic, hydrogen storage and oxidation properties. Mg_3RE (RE: Mm, La, Nd) compounds have recently been studied for their promising hydrogen storage properties [18]. The hydride of the high temperature Laves phase Mg_2Ce was studied by Orgaz [19]: CeM_2H_7 is closely related to the Mg_2Ce intermetallic and has a distorted C-15 cubic structure with interesting electronic properties with the Fermi level cutting the Ce-*f* band leading to possible metallic conduction. The mechanical (elastic moduli) and thermodynamic properties of the C-15 Mg_2Ce Laves phase was recently calculated from first principles by Ouyang et al. [20], it was concluded that the Mg_2Ce would be more ductile than the MgCe and the Mg_3Ce phases. Oxidation studies on the CeMg intermetallic [21] showed that negligible oxidation is observed at room temperature.

The early experimental investigations of the phase diagram conducted in this region have been the 1915 [22] and 1947 [23] studies of Vogel; the results were striking different and both considered rather doubtful because the cerium that was used contained 6.5% impurities. The latter work assumed to be more correct is still used as the existing phase diagram [9] of the Mg–Ce system. The Mg_3Ce region of the phase diagram seems to have been assessed largely based on the expected similarity of the Mg–Ce system to the Mg–La system [11]. A possible composition range at elevated-temperature was postulated for Mg_3Ce which needs further study. Additionally, a Mg_4Ce phase with unknown composition is also mentioned by Raynor [11]. In 2001, Saccone et al. [13] conducted thermal analysis on Ce-rich sample, which confirmed the position of the monovariant curves previously inferred from XRD and metallographic data in the literature.

In 2009, the composition range in the 38–70 wt% was studied by Zhang et al. [2] via EPMA and XRD on Mg–38 wt% Ce and Mg–66 wt% Ce alloys. A metastable μ-Mg_3Ce phase, with the $Mg_{3.0–3.3}Ce$ composition and a possible orthorhombic structure was discovered. The Mg_4Ce phase with the $Mg_{3.6–3.7}Ce$ which was considered to be the vacancy defect structure of Mg_3Ce was also observed. Based on the possible metastability of this phase, it was shown with a dotted line in the suggested phase diagram [2].

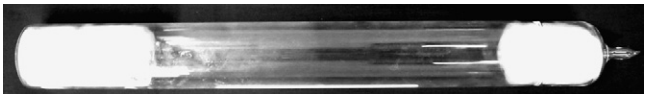

Fig. 1. The Mg–Ce diffusion couple encapsulated in quartz tube.

In order to partially validate the suggested phase diagrams of [1,2], a diffusion couple investigation has been carried out. This paper reports on the results of the diffusion couple and proposes a revised Mg–Ce phase diagram up to 50 at% Ce.

2. Experimental procedures

2.1. Preparation of the diffusion couple

A solid–liquid contact method was employed to produce the Mg–Ce diffusion couple. High purity starting materials were used (Table 1): Mg ingot (99.96%) was supplied by Timminco Metals, Haley, Ontario, Canada; and Ce (99.7%) was supplied by (Hefa Rare Earths Canada Co. Ltd., Richmond, BC, Canada). Analysis by inductively coupled plasma (ICP) at Genitest Labs (Montreal) showed ~0.37 wt% impurities in cerium and 0.02 wt% impurities in magnesium. Fast Neutron Activation Analysis (FNAA) at Texas A&M University was used to detect the oxygen content more precisely especially during manipulation in the laboratory: oxygen levels determined in pure cerium samples that have been exposed to cutting and handling for 30 min were measured to be ~0.7 wt%. This was mainly due to the formation of an oxide scale on the surface.

A rectangular piece of cerium was polished with 320-grit SiC paper under paraffin oil, and then cleaned with acetone to ensure an oxide free surface. Pure magnesium was melted under a protective atmosphere of CO_2 + 0.5% SF_6. The melt was then taken from the furnace under a cover gas of CO_2 + 0.5% SF_6 and cerium was immediately submerged into the molten magnesium. Due to the higher thermal expansion coefficient of magnesium ($26.0 \times 10^{-6}\ K^{-1}$) compared to that of cerium ($8.0 \times 10^{-6}\ K^{-1}$), an intimate contact between magnesium and cerium formed during solidification. The sample was then sectioned and encapsulated in a vacuum quartz tube shown in Fig. 1. A titanium sponge getter was used in case any gas evaporation occurred at high temperature. The quartz tube was placed in a Blue-M mechanical convection furnace, heat treated at 400 °C for 14 days, and then quenched in cold air which shattered the quartz tube and rapidly cooled the diffusion couple.

2.2. Material characterization

The diffusion couple was polished by conventional metallographic technique using diamond paste with an oil-based extender and studied via JEOL840 scanning electron microscopy/energy dispersive spectroscopy (SEM/EDS). Phase identification was further carried out via electron probe microanalysis (EPMA) using a JXA8900L equipped with wavelength-dispersive spectroscopy (WDS) for quantitative analysis.

Table 1
Impurities in cerium (ppm)*.

Impurities in Ce (total impurities 3738 ppm) Rare earths													
La	Pr	Nd	Sm	Eu	Gd	Tb	Dy	Ho	Er	Tm	Lu	Y	Ce
320	150	430	10	2	5	2	5	1	1	1	1	10	Bal
Impurities in Ce (total impurities 3738 ppm) Others													
Si	Fe	C	Ni	Al	Mg	O*	Ca	Ta	Mo	Mn	W	N	
180	1050	450	50	420	50	115	50	50	210	25	100	50	
Impurities in Mg (total impurities 198 ppm)													
Si	Fe	Zn	Ni	Al	Cu	Mn	Ca	O*	Pb	Sn	Cd	Mg	
30	22	40	3	40	2	21	10		10	10	10	Bal.	

* Verified subsequently via FNAA

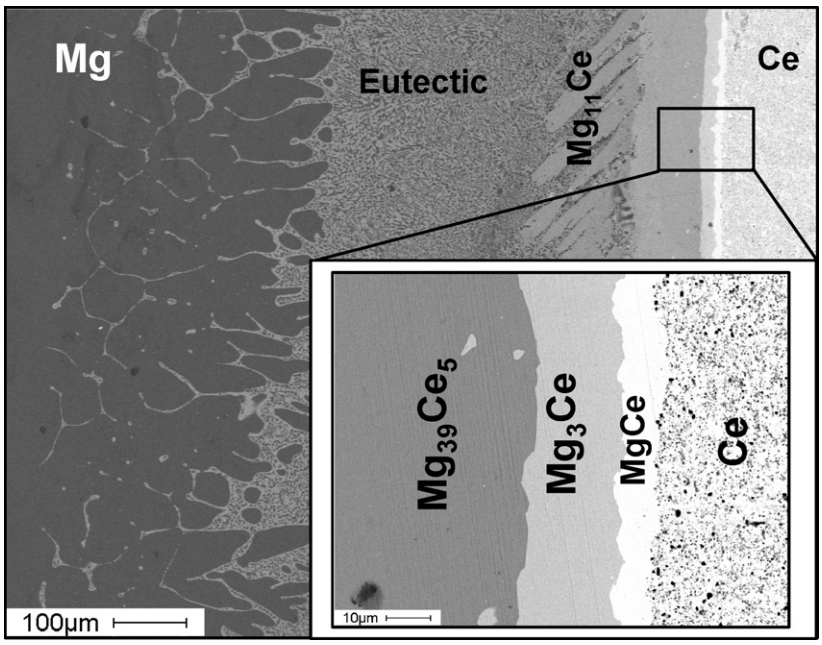

Fig. 2. Diffusion layers formed between Mg and Ce at 400 °C.

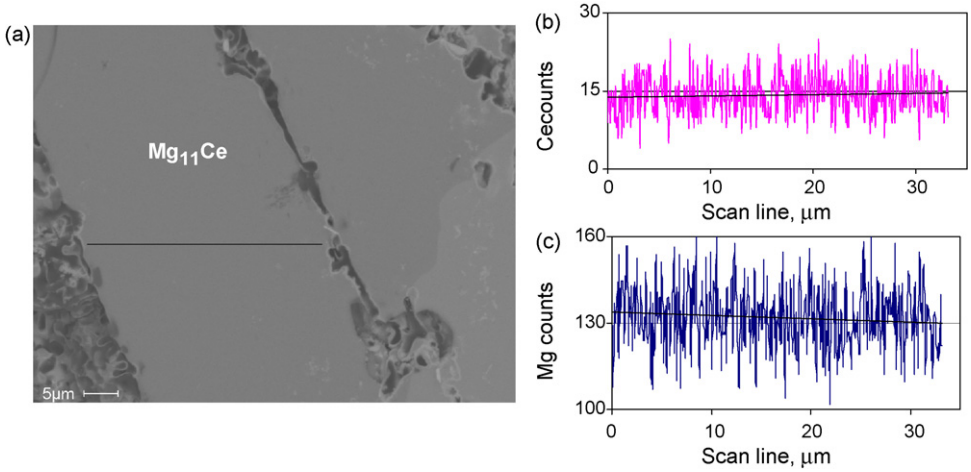

Fig. 3. (a) SEM line scan of the $Mg_{11}Ce$ phase and the EDS spectra showing the compositional variation in (b) Ce and (c) Mg.

3. Results and discussion

SEM image (Fig. 2) shows the different zones formed in the diffusion couple at 400 °C. Five regions are visible from the pure Mg on the left to pure Ce on the right. The thickness of the layers varies from 200 μm to 5 μm owing to the different diffusion coefficients of Mg and Ce atoms.

EPMA indicated that four intermetallic zones formed: $Mg_{11}Ce$, $Mg_{39}Ce_5$, Mg_3Ce, and MgCe. The formation of the eutectic $Mg_{11}Ce$ + Mg zone on the right is due to the solid–liquid method of making the diffusion couple: when the cerium was immersed in molten magnesium, some Ce dissolved, and the eutectic formed on its surface. The columnar $Mg_{11}Ce$ may have formed from the eutectic instead of from the pure Mg, making the shape different from the other three planar layers.

The zones were quantitatively analyzed by EPMA (Table 2). The Mg/Ce ratio confirms the re-designation of $Mg_{12}Ce$ and $Mg_{41}Ce_5$ as $Mg_{11}Ce$ and $Mg_{39}Ce_5$, respectively [1,2]. EPMA indicated an oxygen level of 1–3 at% (increasing towards the Ce side). This does not correlate with the deviation of the measured Mg/Ce ratio of the intermetallics from the theoretical formulae, which is the highest for $Mg_{11}Ce$ and the lowest for Mg_3Ce.

In order to study the solid solution range of the $Mg_{11}Ce$ at 400 °C, SEM line scans were obtained (Fig. 3). Although the Mg and Ce counts fluctuate, the tendency for an increase in cerium and decrease in magnesium can be noted confirming the results obtained previously by Zhang et al. [1]. All other phases, $Mg_{39}Ce_5$, Mg_3Ce and MgCe exhibit near constant Mg/Ce ratio in the interdiffusion zones indicating that these compounds are stoichiometric. The diffusion couple study at 400 °C also shows that the Mg_4Ce

Table 2
EPMA results of the interdiffusion zones in the Mg–Ce diffusion couple.

	Mg (at%)	Ce(at%)	Mg/Ce ratio (std. dev)	Mg/Ce theoretical
$Mg_{11}Ce$	90.10	8.36	10.78 (0.18)	12
$Mg_{39}Ce_5$	87.56	11.39	7.69 (0.05)	8.2
Mg_3Ce	73.24	24.68	2.97 (0.03)	3
MgCe	46.57	48.88	0.95 (0.01)	1

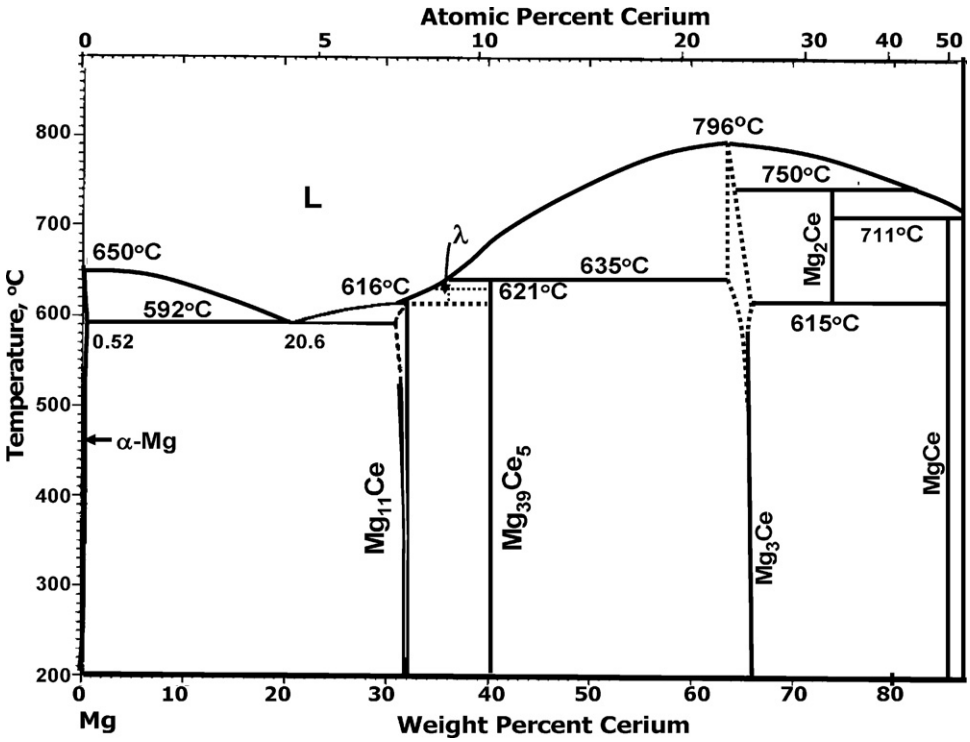

Fig. 4. Revised Mg–Ce phase diagram up to 50 at% Ce.

phase discovered in the previous study [2] is metastable since it does not form under equilibrium conditions at this temperature (though its stability at a higher temperature cannot be entirely ruled out). This study, coupled with the results of the previous investigation [1], allows the authors to propose a revised binary phase diagram for the Mg–Ce system up to 50 at% Ce (Fig. 4). The revised version differs from the existing phase diagram mainly on the Mg-rich side. The $Mg_{11}Ce$ and $Mg_{39}Ce_5$ replace $Mg_{12}Ce$ and $Mg_{41}Ce_5$ as stable and possibly vacancy defect structures. A recent study on the hydrogenation behavior and crystal structure of $Mg_{12}La$ by Denys et al. [24] has re-designated this intermetallic as $Mg_{11}La$ with a giant unit cell and this was associated with the partial substitution of Mg pairs by La atoms in the $Mg_{12}La$ structure at two different crystallographic positions. Based on the similarity between Mg–Ce and Mg–La systems it is possible that $Mg_{11}Ce$ forms similarly via the partial substitution of certain Mg sites with Ce atoms, instead of a vacancy defect structure.

The $Mg_{10.3}Ce$ phase is retained in the phase diagram but is designated as λ because of the difficulty in the previous studies related to understanding this high temperature phase, first as $Mg_{17}Ce_2$ then as a Mg-enriched and non-stoichiometric $Mg_{10.3}Ce$ phase [10]. In fact, Johnson and Smith [25] were not certain of the exact composition of the $Mg_{10.3}Ce$ (Th_2Ni_{17}-type) phase; the formula deduced from a single-crystal structure determination was not considered to accurately reflect the composition of the bulk material. It is also likely that the $Mg_{11}Ce$ phase has extended solid solubility (Ce-enrichment) at high temperatures which may alter the current phase diagram in this interval. Further study is needed to clarify this region of the phase diagram at high temperature; therefore, the λ-compound and the phase boundaries in this region are shown as dotted lines in the suggested phase diagram. The boundaries of the

Table 3
Mg–Ce compounds in the 0–50 at% cerium range [9,1,2].

Formula	Composition at% Ce	Pearson symbol/Prototype	Lattice parameters, (nm)	Comments
Stable phases				
$Mg_{11}Ce$ [1]*	8.1–8.5*	tI26/$Mn_{12}Th$	$a = 1.033$, $c = 0.5964$	Zhang et al. [1]
$Mg_{39}Ce_5$ [2]*	11.3–11.4*	tI92	$a = 1.454$, $c = 1.028$	Temperature range <621 °C
			$a = 1.478$, $c = 1.043$	Vacancy defect structure of $Mg_{41}Ce_5$ [2]
Mg_3Ce [9]	25.0	cF16/BiF3	$a = 0.7428$ or $a = 0.7424$	Temperature range <796 °C
Mg_3Ce [9,2]*	24.0–25.0*	cF16/BiF3	$a = 0.7428$ or $a = 0.7424$	Temperature range <796 °C
Mg_2Ce [9]	33.3	cF24/Cu_2Mg	$a = 0.8733$	Temperature range 615-750 °C
MgCe*	48.9*	cP2/CsCl	$a = 0.3898$, $a = 0.3912$	Temperature range < 715 °C
Metastable phases				
$Mg_{3.6}Ce$ [2]	21.7*	cF16/BiF3	$a = 0.7428$ or $a = 0.7424$	Temperature range <635 °C
				Vacancy defect structure of Mg_3Ce. Metastable*
μ-Mg_3Ce [2]	23.8–25.0*	Orthorhombic [2]	[2]	Metastable
To be confirmed				
λ-$Mg_{10.3}Ce$**	~9–10	hP38/$Ni_{17}Th_2$	[9]	[9,11,12] needs further study

* This study.
** Needs to be verified.

Mg_3Ce phase above 530 °C are also shown as dotted lines in Fig. 4 based on [2].

Table 3 gives a summary of the stable and metastable phases in the Mg–Ce system. The occurrence of the stable $Mg_{11}Ce$ as a possible vacancy defect structure is interesting for Mg alloy development; such a structure would likely form solid solution phases with other elements influencing the thermal/microstructural stability of Mg–Ce based alloys [26]. Indeed in this study, the $Mg_{11}Ce$ phase in the Mg–Mn–Ce alloys show Mn solubility. The existence of a metastable Mg_4Ce phase with the Mg_3Ce structure, which persists after long term annealing [2], is important for hydrogen storage research. The metastable μ-Mg_3Ce phase [2] can be explained as the phase transformation of the lattice-strained D03 (cF16) stable Mg_3Ce phase into metastable orthorhombic oP16 phase. Such transformation has been observed in the D03 (cF16) Fe_3Si compound [27].

The $Mg_{10.3}Ce$ phase (designated as λ by the present authors) is a possible high temperature phase. However, this region of the phase diagram needs further study. The diffusion couple study of [12] utilized only 10 min of annealing at 600 °C; it is possible that complete equilibrium may not have been attained in such a short time. The possible metastability of the phase cannot be ruled out. Future work on the system needs to be conducted (i) to address the controversy around the high temperature $Mg_{10.3}Ce$ ($Mg_{17}Ce_2$) phase as well as (ii) in the high temperature region between 20 and 30 at% Ce to confirm the phase boundaries of Mg_3Ce above 400 °C.

4. Conclusions

1. Electron probe microanalysis of Mg–Ce diffusion couple annealed at 400 °C confirmed the compositions of the four binary intermetallics on the Mg-rich half as $Mg_{11}Ce$, $Mg_{39}Ce_5$, Mg_3Ce, and MgCe.
2. The quantitative EPMA analysis and SEM/EDS line scans showed that $Mg_{11}Ce$ has a narrow composition range with Ce at% ranging from 8.1 to 8.5. On the other hand, $Mg_{39}Ce_5$, Mg_3Ce, and MgCe intermetallics are stoichiometric with near constant Mg/Ce ratio.
3. The Mg_4Ce intermetallic seen in previous work [2] has been confirmed to be metastable.
4. A revised version of the Mg–Ce phases diagram up to 50 at% Ce is proposed, where the $Mg_{11}Ce$ and $Mg_{39}Ce_5$ replace $Mg_{12}Ce$ and $Mg_{41}Ce_5$ as stable and possibly vacancy defect structures.
5. In the revised diagram, the $Mg_{10.3}Ce$ high temperature phase is designated as the λ phase due to the uncertainty detected in the composition and the stability of this phase in previous studies. Consequently, the phase boundaries in the λ region are shown as dashed lines.

Acknowledgements

The authors would like to thank Mr. Pierre Vermette for the challenging work in making the diffusion couple. The financial support of Natural Sciences and Engineering Research Council (NSERC) of Canada, General Motors of Canada and McGill University are acknowledged.

References

[1] X. Zhang, D. Kevorkov, M. Pekguleryuz, J. Alloys Compd. 475 (2009) 361–367.
[2] X. Zhang, D. Kevorkov, M. Pekguleryuz, Intermetallics 17 (2009) 496–503.
[3] M.O. Pekguleryuz, A.A. Kaya, Adv. Eng. Mater. (2003) 866–878, DGM, l. 5.
[4] A. Luo, M.O. Pekguleryuz, J. Mater. Sci. 29 (1994) 313–319.
[5] A. Luo, J. Int. Mater. Rev. 49 (1) (2004) 13–30.
[6] K.H.J. Buschow, J. Less-common Met. 44 (1976) 301.
[7] R. Ferro, S. Delfino, G. Borzone, A. Saccone, G. Cacciamani, J. Phase Equilib. 14 (3) (1993).
[8] J. Zhang, P. Yu, K. Liu, D. Fang, D. Tang, J. Meng, Mater. Des. 30 (2009) 2372–2378.
[9] T.B. Massalski (Ed.), Binary Alloy Phase Diagrams, 2nd ed., ASM International, Materials Park, Ohio, 1990.
[10] L.L. Rokhlin, Magnesium Alloys Containing Rare Earth Metals: Structure and Properties, Taylor & Francis, 2003.
[11] G.V. Raynor, The Physical Metalurgy of Magnesium and its Alloys, Pergamon press Ltd, 1959.
[12] D.H. Wood, E.M. Cramer, J. Less-common Met. 9 (1965) 321–337.
[13] A. Saccone, D. Macciò, S. Delfino, F. Hayes, R. Ferro, J. Therm. Anal. Calorim. 66 (2001) 47–57.
[14] A.A. Nayeb-Hashemi, J.B. Clark, Phase Diagrams of Binary Magnesium Alloys, ASM, Metals Park, OH, 1988.
[15] R.E. Smallman, R.J. Bishop, Modern Physical Metallurgy and Materials Engineering, 6th Ed., Butterworth-Heinemann, 1999.
[16] D.W. Zhou, P. Peng, J.S. Liu, J. Alloys Compd. 428 (2007) 316–321.
[17] F. Grandjean, G.D. Waddill, T.R. Cummins, D.P. Moore, J. Long S Gary, K.H.J. Buschowc, Solid State Commun. 108 (8) (1998) 593–597.
[18] L.Z. Ouyang, H.W. Dong, C.H. Peng, L.X. Sun, M. Zhu, Int. J. Hydrogen Energy 32 (2007) 3035–3929.
[19] E. Orgaz, J. Alloys Compd. 322 (2001) 45–54.
[20] Y. Ouyang, X. Tao, H. Chen, Y. Feng, Y. Du, Y. Liu, Comp. Mater. Sci. 47 (2009) 297–301.
[21] B. Stumpy, Y. Mudryk, A. Russell, D. Herman, K. Gschneidner Jr., J. Alloys Compd. 460 (2008) 363–367.
[22] R. Vogel, Z. Anorg. Chem. 91 (1915) 277.
[23] R. Vogel, T. Heumann, Metallforschung 2 (1947) 1–8.
[24] R.V. Denys, A.A. Poletaev, J.K. Solberg, B.P. Tarasov, V.A. Yartys, Acta Mater. 58 (2010) 2510–2519.
[25] Q. Johnson, G.S. Smith, Acta Cryst. B26 (1970) 434–435.
[26] X. Zhang, D. Kevorkov, I.-H. Jung, M. Pekguleryuz, J. Alloys Compd. 482 (2009) 420–428.
[27] M. Mihalkovic, M. Widom, Phys. Rev. B 70 (2004) 1–12.